ARL-TR-8788 ● SEP 2019

Automated Flight Control Design for Guided Munitions

by Luisa Fairfax

NOTICES

Disclaimers

The findings in this report are not to be construed as an official Department of the Army position unless so designated by other authorized documents.

Citation of manufacturer's or trade names does not constitute an official endorsement or approval of the use thereof.

Destroy this report when it is no longer needed. Do not return it to the originator.

ARL-TR-8788 ● SEP 2019

Automated Flight Control Design for Guided Munitions

by Luisa Fairfax
Weapons and Materials Research Directorate, CCDC Army Research Laboratory

REPORT DOCUMENTATION PAGE

Form Approved
OMB No. 0704-0188

1. REPORT DATE *(DD-MM-YYYY)*	2. REPORT TYPE	3. DATES COVERED (From - To)
September 2019	Technical Report	1 June 2017–1 September 2019

4. TITLE AND SUBTITLE
Automated Flight Control Design for Guided Munitions

5a. CONTRACT NUMBER

5b. GRANT NUMBER

5c. PROGRAM ELEMENT NUMBER

6. AUTHOR(S)
Luisa Fairfax

5d. PROJECT NUMBER

5e. TASK NUMBER

5f. WORK UNIT NUMBER

7. PERFORMING ORGANIZATION NAME(S) AND ADDRESS(ES)
CCDC Army Research Laboratory
ATTN: FCDD-RLW-LE
Aberdeen Proving Ground, MD 21005

8. PERFORMING ORGANIZATION REPORT NUMBER
ARL-TR-8788

9. SPONSORING/MONITORING AGENCY NAME(S) AND ADDRESS(ES)

10. SPONSOR/MONITOR'S ACRONYM(S)

11. SPONSOR/MONITOR'S REPORT NUMBER(S)

12. DISTRIBUTION/AVAILABILITY STATEMENT
Approved for public release; distribution is unlimited.

13. SUPPLEMENTARY NOTES

14. ABSTRACT
The objective of this effort is to efficiently design flight controllers for different vehicle configurations to satisfy performance requirements. Optimal control and linear system analysis techniques are applied to a demonstration vehicle consisting of onboard inertial sensors and four independently actuated canards. The controller gains are automatically computed using pole placement with the linearized system dynamics and desired rise time, settling time, and overshoot. Linear and nonlinear controlled flight simulations were performed with control gains determined using the automated routine. Results show the utility of this method and quantifies how well the linearization characterizes the nonlinear system dynamics.

15. SUBJECT TERMS
optimal control, automatic tuning, linear analysis, pole placement, precision projectile, second-order response

16. SECURITY CLASSIFICATION OF:			17. LIMITATION OF ABSTRACT	18. NUMBER OF PAGES	19a. NAME OF RESPONSIBLE PERSON
a. REPORT	b. ABSTRACT	c. THIS PAGE			Luisa Fairfax
Unclassified	Unclassified	Unclassified	UU	21	19b. TELEPHONE NUMBER (Include area code) 410-306-2104

Contents

List of Figures

List of Tables

Acknowledgments

Thank you to Dr Frank Fresconi for his ideas and input on this research and for reading and reviewing the first draft of the manuscript. His contributions are much appreciated.

1. Introduction

The need to more effectively guide munitions with novel and low-cost component technologies is what motivated this research. Past work (Fresconi et al. 2014a, 2014b, 2015) developed nonlinear and linearized models of flight used in an optimal control formulation for an aerodynamically controlled munition with inertial sensor feedback. The weightings for the control effort and feedback state errors are used along with the linear system dynamics to obtain the gains within the linear quadratic regulator framework. The system dynamics, and hence the optimal control gains, change based on flight conditions to include Mach number and trim angle of attack. Tuning this controller across flight conditions by hand is labor intensive. Fortunately, methods such as pole placement (Franklin et al. 1986) can be applied within a numerical routine to automate this process. A set of desired performance metrics, which includes rise time, settling time, and percent overshoot is needed for this method. This approach was recently applied to improve the control performance of a low-cost servo-mechanism (Burchett 2017).

This report outlines the flight dynamics and control prior to extending the control techniques to automatic gain selection. The controllers found by this method were implemented in nonlinear Monte Carlo simulations to assess the suitability of the automated linear control analysis for this vehicle class. Further adoption of this methodology across Mach number and trim angle of attack is discussed.

2. System Dynamics and Optimal Control

The nonlinear and linearized dynamics of the system can be found in Fresconi et al. (2014b). The block diagram for the optimum controller is shown in Fig. 1, where Gp is the plant dynamics and can include in series the actuator and flight dynamics. The optimal control gains that will be solved for is K.

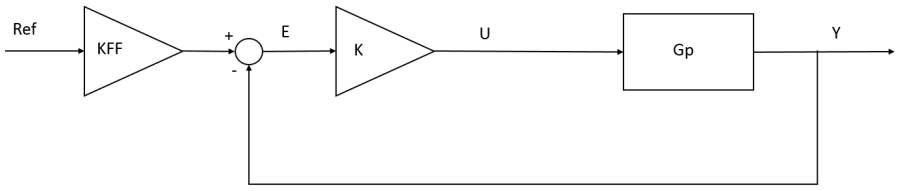

Fig. 1 Block diagram for optimum control system

The states that are controlled are roll angle (ϕ), roll rate (p), pitch rate (q), yaw rate (r), and lateral accelerations (a_j, a_k). The reference vector is thus $X_{REF} = \lfloor \phi_{REF} \quad p_{REF} \quad q_{REF} \quad r_{REF} \quad a_{j,REF} \quad a_{k,REF} \rfloor$. There are three controls,

$\delta_p, \delta_q, \delta_r$, in the roll, pitch, and yaw channels, respectively, which are then used to calculate the resulting control commands for the four canards based on the roll orientation of the canards. The optimum controller is developed by minimizing the cost function (J) as shown in Eq. 1.

$$J = \int_0^\infty \left(X^T Q X + U^T R U \right) dt, \tag{1}$$

where X is the state, Q and R are matrices weighting the state feedback error and control effort, U is the control, and t is time. The resulting optimum controller is shown in Eq. 2.

$$U = -K(X - X_{REF}). \tag{2}$$

The gain matrix is found using

$$\dot{X} = AX + BU, \tag{3}$$

$$K = R^{-1} B^T P, \tag{4}$$

and

$$A^T P + PA - PBR^{-1} B^T P + Q = 0, \tag{5}$$

where A is the linearized state transition matrix, B is control matrix, and P is found using the algebraic matrix Riccatti equation as shown. Next, we derive the automated method through which the gain K is found using a pole placement strategy.

3. Pole Placement for Desired Response Given System Dynamics

Selection of the gains is determined using a pole placement strategy based on the linear system dynamics and desired response. The poles closest to the imaginary axis will dominate the response and the system is required to be stable (no real poles). The closed-loop transfer function and poles are as shown.

$$G_{CL}(s) = \frac{\omega_n^{\,2}}{s^2 + 2\varsigma\omega_n s + \omega_n^2}, \tag{6}$$

and

$$p = -\varsigma\omega_n \pm j\omega_n\sqrt{1-\varsigma^2}, \tag{7}$$

where $G_{CL}(s)$ is the approximate second-order response of the system, p are the poles, ς is the system damping, and ω_n is the system natural frequency. The calculations result in the following eigenvalue requirements (Burchett 2010):

$$\zeta = -\frac{\ln\left(\%\frac{OS}{100}\right)}{\sqrt{\pi^2+\ln\left(\%\frac{OS}{100}\right)^2}}, \tag{8}$$

$$\theta < \tan^{-1}\left(\frac{\sqrt{1-\zeta^2}}{-\zeta}\right), \tag{9}$$

$$\sigma_{ts} > \frac{4}{t_s}, \tag{10}$$

and

$$\omega_n \geq \frac{1.8}{t_R}, \tag{11}$$

where the design parameters are percent overshoot (%OS), settling time (t_s), and rise time (t_r). These design parameters result in eigenvalue placement within the angle θ, settling time real value r_{ts}, and rise time real value r_{tr}. $\omega_{d,tr}$ is the damped frequency, and it is the value of the imaginary component of the dominant eigenvalue (Nise 2015).

The optimum gain K is determined by adjusting the Q and R weighting matrices. Increasing Q increases the penalty on state feedback error and increasing R increases the penalty on control effort. The weighting matrix for state feedback error includes terms for each feedback state. Roll, pitch, and yaw channels are first isolated to compute gains that are used to initialize the process for the full system dynamics. The roll channel reference states are $X_{REF} = [\phi_{REF} \quad p_{REF}]$ and correspond with rows 1 and 2 and columns 1 and 2 of the dynamic matrix A (see Eq. 5). The pitch and yaw channel reference states are $X_{REF} = \lfloor q_{REF} \quad a_{j,REF} \rfloor$ and $X_{REF} = \lfloor r_{REF} \quad a_{k,REF} \rfloor$, respectively. They correspond with dynamic matrix columns 3 and 6 and 4 and 5, respectively. This procedure is also initially performed considering only the flight dynamics before conducting the analysis with the combined flight and actuator dynamics.

The algorithm is as follows:

Algorithm: Pole Placement

1) Initialize Q and R as follows. Q components for the tracking rate are set to the area in which the tracking weight is expected to be for each component. Randomly generated permutations are run until one with the lowest cost function is found. The cost function is defined to be stable and having the best percent design characteristics. R is the identity multiplied by the model weight with the model weight of R_weight = 10, and Q_weight = 0.005. If the system fails stability, increase Q_phi.

2) Compute linearized system dynamics matrices at given flight condition (e.g., Mach number, trim angle of attack).

3) For each roll (phi, phidot), pitch (pitch rate, pitch acceleration), and yaw (yaw rate, yaw acceleration), do the following independently:

   a. Solve for K using LQR $\begin{aligned} K &= R^{-1}B^T P \\ A^T P + PA - PBR^{-1}B^T P + Q &= 0 \end{aligned}$.

   b. Compute closed-loop eigenvalues.

   c. Check that eigenvalues are within angle, imaginary and real value requirements derived from design parameters (Eqs. 9–12).

   d. If requirements are not satisfied, increase weight for this parameter by multiplying Q_weight = Q_weight × 1.1.

   e. If positive real eigenvalues or Q_weight > 10, terminate with message requiring relaxation of requirements.

4) If a stable Q is found, then repeat Steps a–e with full system dynamics. If a stable Q is not found, start over with Step 1 using a different randomly generated Q.

4. Linear Response Analysis

Linear results from the automated gain selection method are presented next. The design requirements were 4.5% maximum percent overshoot, 1 s maximum 2% settling time, and minimum rise time of 0.02595 s. For comparison, the design requirements were relaxed by a factor of two to 9% maximum percent overshoot, 2 s maximum settling time, and a minimum rise time of 0.0519 s.

The poles were placed as shown in Figs. 2 and 3. To show the trend as Q is increased, the initial poles are plotted in green, intermediate poles are plotted in gray, and the final poles are plotted in red. Pitch and yaw eigenvalues are the same as the projectile is symmetric.

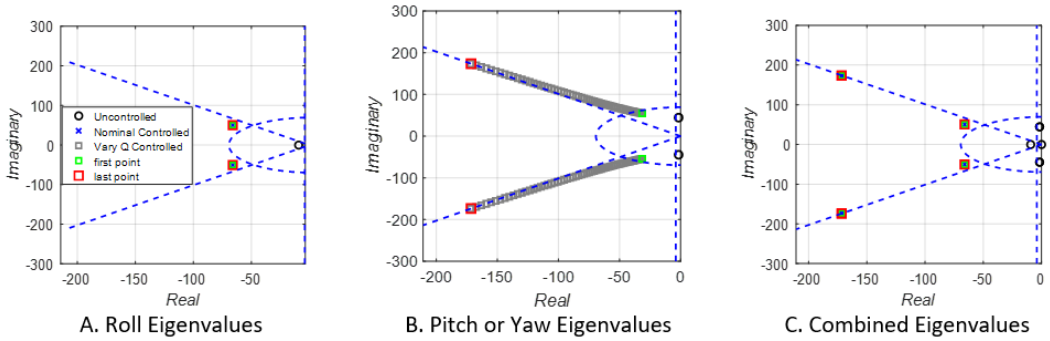

Fig. 2 Linear flight dynamic eigenvalue placement

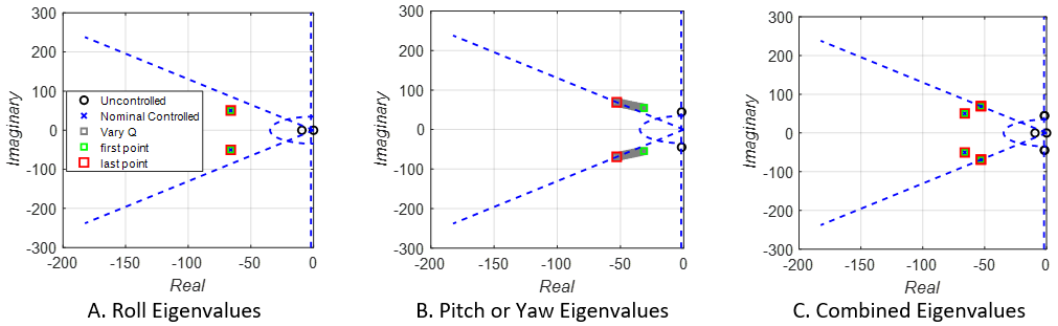

Fig. 3 Linear flight dynamic eigenvalue placement, relaxed requirements by a factor of 2

The projectile is governed by flight dynamics and also actuator dynamics. The actuator dynamics change the overall system plant and most be considered in the controller and system response as shown in the series block diagram (Fig. 4).

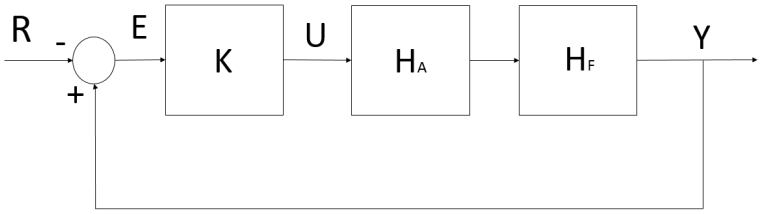

Fig. 4 Block diagram of linear system with feedback gain K, actuator plant H_A, and flight plant H_F

The actuator dynamics are modeled as first-order system with a time delay and bias as shown in Eq. 12. Details are found in Fresconi et al. (2014a).

$$\tau\dot{\delta}(t) + \delta(t) = \delta_c(t - t_D) + \delta_B \tag{12}$$

The first-order, linear actuator model is as shown in Eqs. 13 and 14 with the corresponding transfer function.

$$\tau\,\dot{\delta} + \delta = \delta_C \ . \tag{13}$$

$$H_A(s) = e^{-t_D s}\frac{1/\tau}{s + 1/\tau} \ . \tag{14}$$

The flight dynamics alone assume that the control does not have to be applied to the actuator dynamics. In reality, the actuator dynamics contribute to the dynamics of the overall system. The actuator dynamics alone are plotted in Fig. 5 and show the actuator poles that will contribute to the overall closed-loop system. In the following analysis, the delay will be assumed to be very small, less than 1 ms. Incorporating second-order actuator dynamics without time delay, the tuning is done as follows. Results are as shown in Figs. 6 and 7.

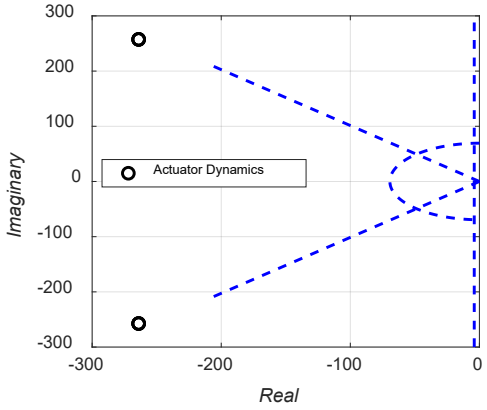

Fig. 5 Actuator dynamics

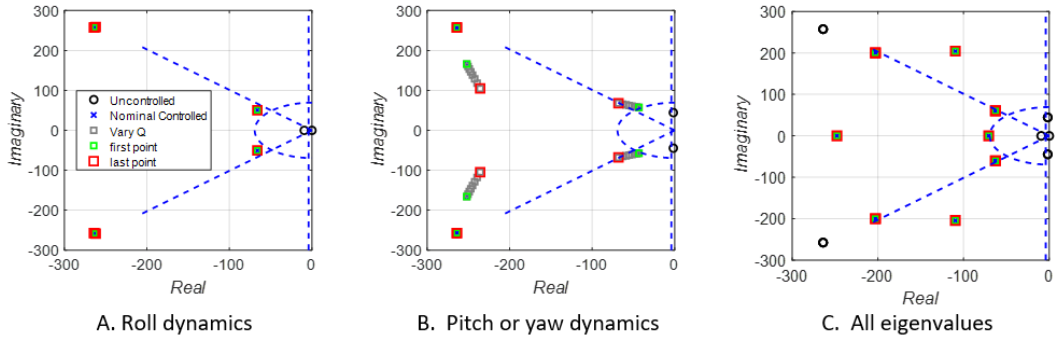

Fig. 6 Eigenvalue placement with second-order actuator dynamics

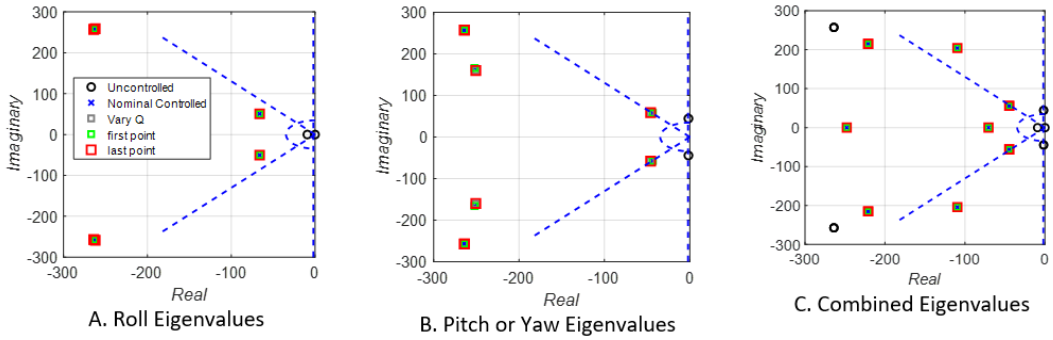

Fig. 7 Eigenvalue placement with second-order actuator dynamics, relaxed requirements by a factor of 2

The linear step time responses for the flight dynamics and system dynamics are provided in Figs. 8 and 9. They represent the ideal case of a second-order controller applied to a linear system.

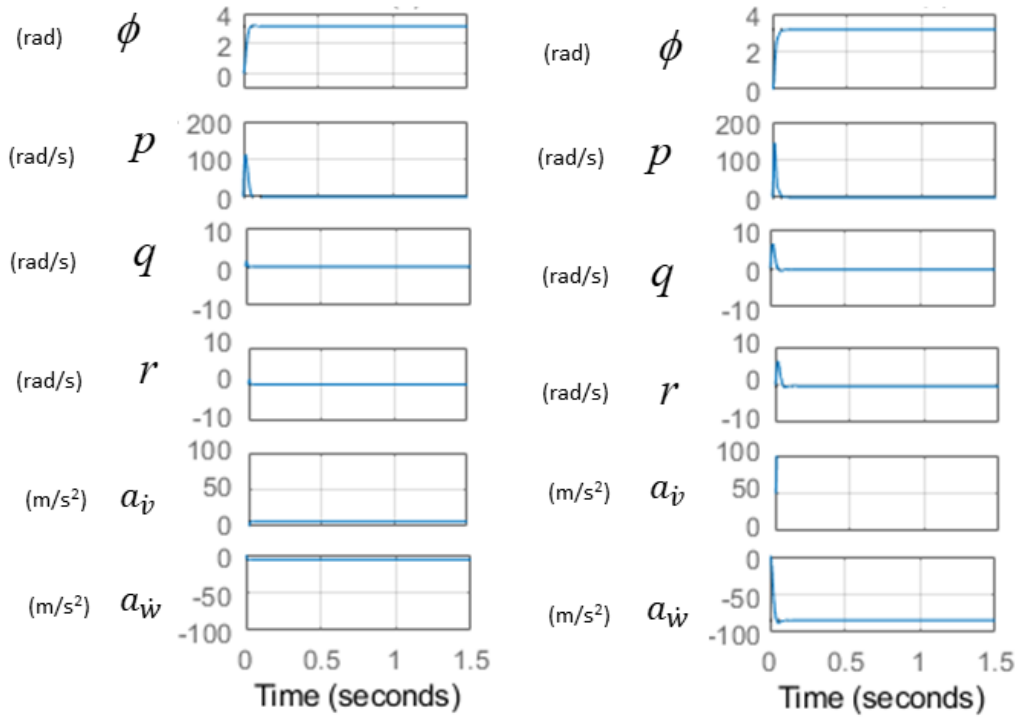

a) Flight Dynamics Only b) Flight & Actuator Dynamics

Fig. 8 Ideal linear step response performed by activating the corresponding canard into a step on the linear transfer function

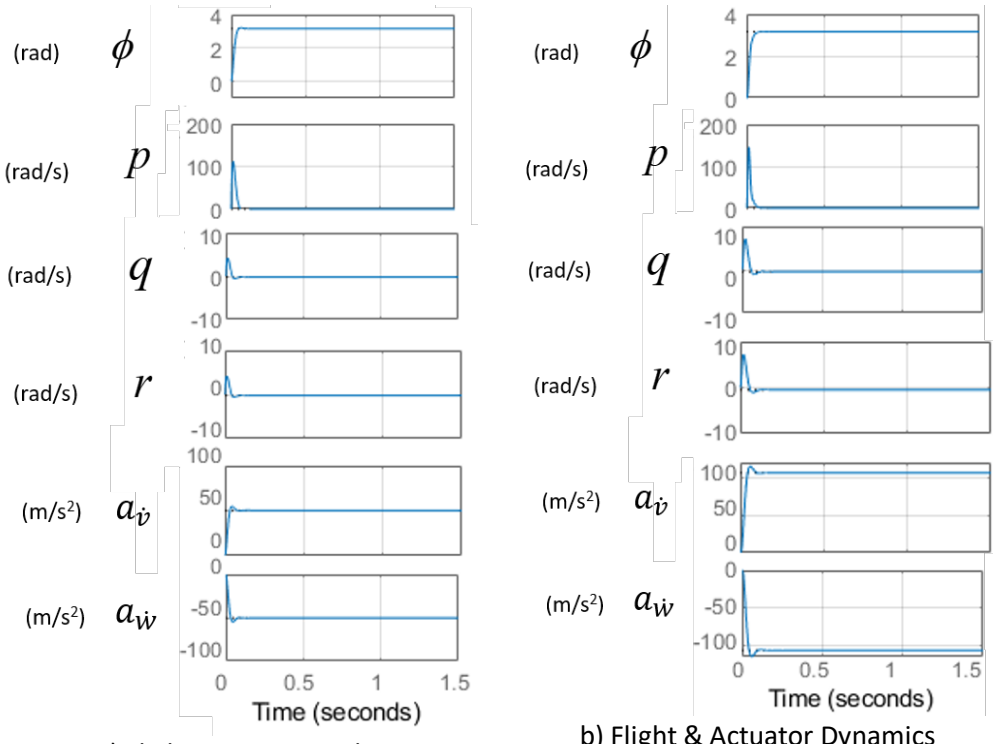

a) Flight Dynamics Only b) Flight & Actuator Dynamics

Fig. 9 Ideal linear step response performed by activating the corresponding canard into a step on the linear transfer function, relaxed requirements by a factor of 2

The corresponding performance requirements are in Table 1. The states and initial conditions are the following:

$$[x \quad y \quad z \quad \phi \quad \theta \quad \psi \quad u \quad v \quad w \quad p \quad q \quad r] =$$
$$[0m \quad 0m \quad 0m \quad 10° \quad 7.55° \quad 0° \quad 225m/s \quad 0m/s \quad 0m/s \quad 2.6Hz \quad -0.22Hz \quad 25Hz].$$

Table 1 shows the performance metrics that result from tuning using the flight dynamics only.

Table 1. Performance metrics from linear step response: flight dynamics only

	Overshoot (%)	Rise time (s)	2% settling time (s)
ϕ	0	0.0314	0.0630
p	0[a]	1.261e-15	0.0687
q	0.1534[a]	0.0019	0.1049
r	0.1534[a]	0.0019	0.1049
a_j	8.230	0.0268	0.0882
a_k	8.230	0.0268	0.0882

[a] percentage is percentage of initial condition (as steady-state value is zero)
Note: Highlights indicate design requirements that were not too stringent and could not be met with this controller and dynamic system.

Next, the full system with the actuator dynamics, in addition to the flight dynamics, was evaluated. The step response for the flight dynamics plus actuator dynamics are shown in Table 2. As in Table 1, the desired metrics are met. The linear step response behaves well. The unachievable parameters are highlighted, indicating that using the dominant poles alone requires some relaxation of the desired parameters. The symmetry between the pitch and yaw angular rates and accelerations are preserved in the linear representation, as there is no gravity. Because the final steady-state value of the rates is zero, the percent overshoot is instead calculated as a percentage of the initial condition ($OS = \frac{abs(x_{OS})}{x_{initial}} 100$).

Table 2. Performance metrics from linear step response: flight and actuator dynamics only

	Overshoot (%)	Rise time (s)	2% settling time (s)
ϕ	1.621	0.0295	0.0448
p	0[a]	1.095e-17	0.0577
q	12.88[a]	2.4516e-04	0.0821
r	12.88[a]	2.452e-4	0.0821
a_j	8.971	0.0216	0.0685
a_k	8.971	0.0216	0.0685

[a] percentage is percentage of initial condition (as steady-state value is zero)
Note: Unachievable parameters are highlighted.

5. Nonlinear Response Analysis

Next, the automatic gain computation routine is evaluated on the nonlinear system dynamics. First, an example of what occurs when the actuator dynamics are not modeled in linear analysis is shown in Fig. 10. The actuator dynamics dominate the response, and the pitch and yaw rates do not converge. This demonstrates the importance of including the actuator dynamics in the controller. The nonlinear response performance metrics with flight dynamics only in the linear analysis are shown in Table 3. The majority of the parameters do not converge. The results are shown in Fig. 11 for a reference command of $X_{REF} = [0^{\circ} \quad 0Hz \quad 0Hz \quad 0Hz \quad 30m/s^2 \quad 1m/s^2]$. The nonlinear simulation was run for 1.5 s, and the steady-state value was taken at t = 1.5 s. The four canard deflections are calculated from the roll, pitch, and yaw controls as shown in Fresconi et al. (2014a).

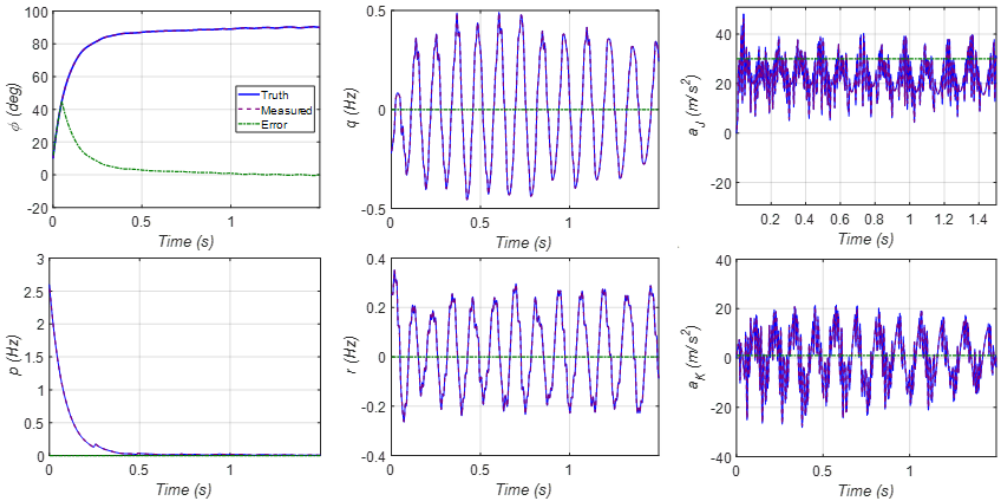

Fig. 10 Tuning including only flight dynamics; tuning without actuator dynamics results in unstable nonlinear response

Table 3 Performance metrics from nonlinear step response: flight dynamics only

	Overshoot (%)	Rise time (s)	2% settling time (s)
ϕ	0	0.1665	0.7885
p	0	0.178	0.364
q	NA[a]	NA[a]	NA[a]
r	NA[a]	NA[a]	NA[a]
a_j	NA[a]	NA[a]	NA[a]
a_k	NA[a]	NA[a]	NA[a]

[a] Did not converge using this method
Note: Highlights indicate unachievable requirements.

Next, the full system with the actuator dynamics in addition to the flight dynamics was evaluated. The responses are plotted in Fig. 11. Although each response converges, not all performance metrics are met. The nonlinear response for the flight dynamics plus actuator dynamics are as shown in Table 4. Unmet performance metrics are highlighted.

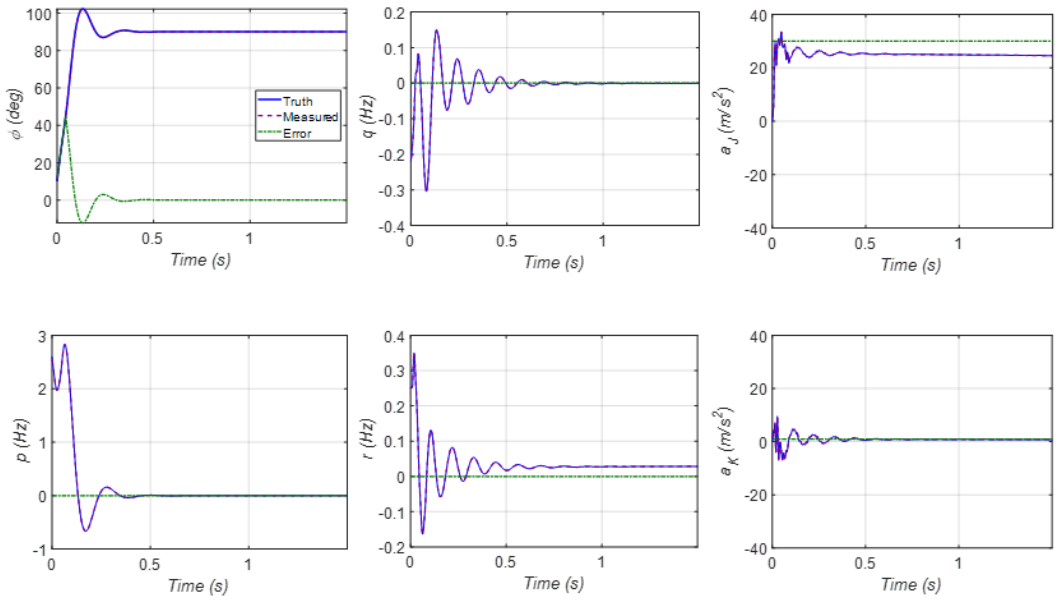

Fig. 11 Controlled maneuver with four canards tuning including actuator dynamics

Table 4 Performance metrics from nonlinear step response: flight and actuator dynamics only

	Overshoot (%)	Rise time (s)	2% settling time (s)
ϕ	13.56	0.072	0.2715
p	25.72[a]	0.036	0.326
q	63.26[a]	0.01605	0.7525
r	56.77[a]	0.012	0.6375
a_j	3.030	0.0073	0.6375
a_k	798.7	0.00091	1.012

[a] percentage is percentage of initial condition (as steady-state value is zero)
Note: Unmet performance metrics are highlighted.

Monte Carlo simulations with a sample size of 100 were conducted with the following variation in initial conditions:

$$\sigma = [1m \quad 1 \quad 1 \quad 6.28rad \quad 0.004 \quad 0.0054 \quad 8.30\,m/s \quad 0 \quad 0 \quad 0.5rad/s \quad 0.5 \quad 0.5].$$

Results are shown in Fig. 12. The average performance metrics from the nonlinear Monte Carlo simulations are shown in Table 5. Recall that the design requirements were 4.5% maximum percent overshoot, 1 s maximum 2% settling time, and minimum rise time of 0.0173 s. These results indicate that the performance can be tuned using a second-order approximate response, but the desired second-order response may not be reached using the nonlinear, combined system. Although the linear system closely represents the second-order system and is able to achieve the desired response, the nonlinear system is instead representative of the best scenario. The roll, roll rate, pitch, and yaw meet the majority of the criteria except for the highlighted cases. The accelerations are the most nonlinear components and they are controlled to a small value, making the percent overshoots high. The rise and settling times also do not match the linear and desired responses due to the control modeling differences and nonlinearities. The previous results show that it is possible to tune a system automatically at a desired trim and Mach number to get a best possible result, but the nonlinear result may not be exactly as desired. In the nonlinear system, the overturning because of acceleration due to gravity also contributed to the non-steady-state response. Another cause for modeling error is that there are actually four canard deflections instead of three, and the canard deflections are not directly related to the roll, pitch, and yaw, but instead are calculated from the roll, pitch, and yaw commands. Roll angle is symmetric, about 90°.

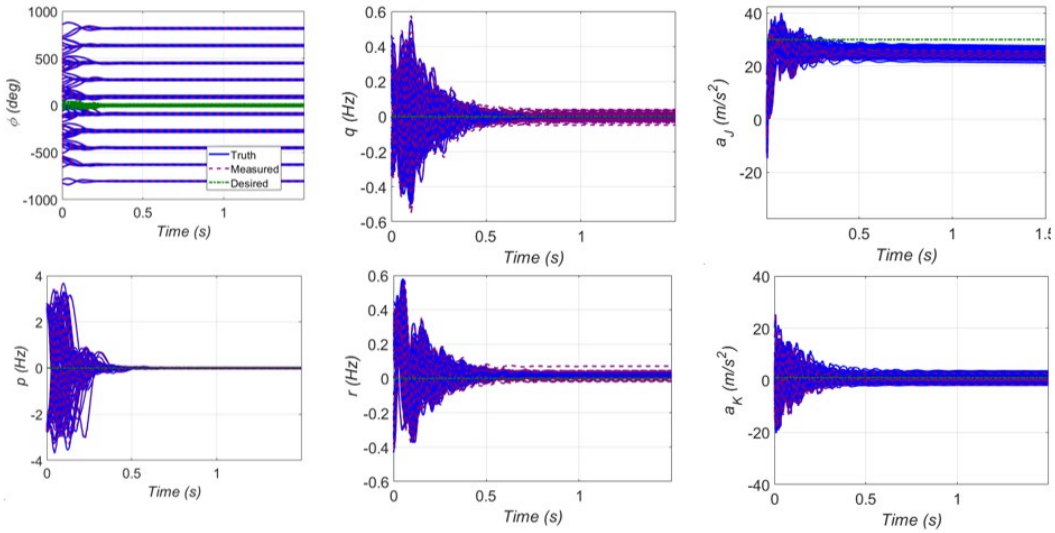

Fig. 12 Monte Carlo of controlled maneuver states with four canards

Table 5 Performance metrics from nonlinear Monte Carlo simulations

	Overshoot (%)	Rise time (s)	2% settling time (s)
ϕ	31.81	0.06786	0.1799
p	46.46	0.07478	0.3649
q	268.1	0.01734	0.8138
r	237.6	0.01765	1.500
a_J	110.7	0.02493	0.8013
a_K	3441	0.007805	1.152

Note: highlights indicate unachievable design parameters.

The current analysis was evaluated over a single Mach number and trim angle of attack condition and resulted in the optimum control gain K. If flying over various flight conditions, the automatic gain selection tool can be run with the appropriate system dynamics obtained from aerodynamic and actuator characterization for scheduling gains.

6. Conclusion

The precision projectile optimum controller can be automatically tuned to attempt to meet second-order design characteristics. Linear analysis is used to place poles and is performed to develop the optimum controller at a specific Mach regime and trim condition. The linear results closely match the desired parameters. The nonlinear results are reasonable but may not fit the design constraints with varying initial conditions. Pole placement is performed for a highly maneuverable airframe precision projectile. Future work will address how to design a projectile profile over a given flight through various regimes to optimize lift over drag. Future work will also address the use of a genetic algorithm to initialize Q.

7. References

Burchett, BT. Dynamic modeling and simulation. Morrisville (NC): Lulu.com; 2010.

Burchett, BT. Matlab tools for automated system identification and control design for SISO motor loops. Aberdeen Proving Ground (MD): Army Research Laboratory (US); 2017. Report No.: ARL-CR-081.

Franklin F, Powell JD, Emami-Naeini A. Feedback control of dynamic systems. Reading (MA): Addison-Wesley; 1986. (Addison-Wesley series in electrical engineering).

Fresconi F, Celmins I, Ilg M, Maley J. Projectile roll dynamics and control with low-cost maneuver system. J Spacecraft Rockets. 2014a;51(2):624–627.

Fresconi F, Celmins I, Silton SI. Theory, guidance, and flight control for high maneuverability projectiles. Aberdeen Proving Ground (MD): Army Research Laboratory (US); 2014b. Report No.: ARL-TR-6767.

Fresconi F, Celmins I, Silton S, Costello M. High maneuverability projectile flight using low cost components. Aerosp Sci Technol. 2015;41:175–188.

Nise NS. Control systems engineering. 7th ed. Hoboken (NJ): Wiley; 2015.

1 (PDF)	DEFENSE TECHNICAL INFORMATION CTR DTIC OCA
1 (PDF)	CCDC ARL FCDD RLD CL TECH LIB
1 (PDF)	GOVT PRINTG OFC A MALHOTRA
1 (PDF)	CCDC ARL FCDD RLW LE L FAIRFAX